

1 **Geological processes mediate a subsurface microbial loop in the deep biosphere**

2

3 Daniel A. Gittins<sup>1\*</sup>, Pierre-Arnaud Desiage<sup>2</sup>, Natasha Morrison<sup>3</sup>, Jayne E. Rattray<sup>1</sup>, Srijak  
4 Bhatnagar<sup>1</sup>, Anirban Chakraborty<sup>1</sup>, Jackie Zorz<sup>1</sup>, Carmen Li<sup>1</sup>, Oliver Horanszky<sup>1</sup>, Margaret A.  
5 Cramm<sup>1†</sup>, Jamie Webb<sup>4</sup>, Adam MacDonald<sup>3</sup>, Martin Fowler<sup>4</sup>, D. Calvin Campbell<sup>2</sup>, and Casey R.  
6 J. Hubert<sup>1</sup>

7

8 <sup>1</sup>Geomicrobiology Group, Department of Biological Sciences, University of Calgary; Calgary,  
9 Canada.

10 <sup>2</sup>Natural Resources Canada, Geological Survey of Canada-Atlantic; Dartmouth, Canada.

11 <sup>3</sup>Department of Energy and Mines, Government of Nova Scotia; Halifax, Canada.

12 <sup>4</sup>Applied Petroleum Technology; Calgary, Canada.

13 <sup>†</sup>Present address: Queen Mary University of London; London; England.

14 **Summary paragraph**

15 The deep biosphere is the largest microbial habitat on Earth and features abundant bacterial  
16 endospores<sup>1,2</sup>. Whereas dormancy and survival at theoretical energy minima are hallmarks of  
17 subsurface microbial populations<sup>3</sup>, the roles of fundamental ecological processes like dispersal and  
18 selection in these environments are poorly understood<sup>4</sup>. Here we combine geophysics,  
19 geochemistry, microbiology and genomics to investigate biogeography in the subsurface, focusing  
20 on bacterial endospores in a deep-sea setting characterized by thermogenic hydrocarbon seepage.  
21 Thermophilic endospores in permanently cold seabed sediments above petroleum seep conduits  
22 were correlated with the presence of hydrocarbons, revealing geofluid-facilitated cell migration  
23 pathways originating in deep oil reservoirs. Genomes of thermophilic bacteria highlight  
24 adaptations to life in anoxic petroleum systems and reveal that these dormant populations are  
25 closely related to oil reservoir microbiomes from around the world. After transport out of the  
26 subsurface and into the deep-sea, thermophilic endospores re-enter the geosphere by  
27 sedimentation. Viable thermophilic endospores spanning the top several metres of the seabed  
28 correspond with total endospore counts that are similar to or exceed the global average. Burial of  
29 dormant cells enables their environmental selection in sedimentary formations where new  
30 petroleum systems establish, completing a geological microbial loop that circulates living biomass  
31 in and out of the deep biosphere.

32 **Main text**

33 Identifying natural forces that distribute organisms throughout the living world is critical to  
34 understanding Earth system functioning. Whereas the biogeography of animals and plants have  
35 been studied since the time of Darwin<sup>5</sup>, related ecological processes are harder to elucidate in the  
36 microbial realm where the effects of dispersal and environmental selection must be disentangled<sup>6–</sup>  
37 <sup>8</sup>. Dormant populations of microbes retain viability while enduring inhospitable conditions in  
38 relation to growth requirements, allowing dispersal to be studied directly without the influence of  
39 conflating factors like environmental selection. Bacterial endospores are equipped to survive  
40 dispersal over long distances and timescales<sup>9</sup>, with reports of viable spores ~2.5 km beneath the  
41 seafloor<sup>10</sup> suggesting dispersal journeys lasting millions of years. This points to a genetically and  
42 functionally diverse seed bank of microbes that can be revived if subsurface environmental  
43 conditions select for their traits<sup>11,12</sup>.

44

45 The marine subsurface biosphere contains an estimated  $10^{29}$  microbial cells contributing up to 2%  
46 of the total living biomass on Earth<sup>1</sup>. Whereas deep biosphere populations exhibit exponentially  
47 decreasing numbers with depth<sup>13</sup>, endospores experience less pronounced declines and appear to  
48 outnumber vegetative cells in deeper marine sediments<sup>2,14</sup>. Measurements of the endospore-  
49 specific biomarker dipicolinic acid indicate remarkably high numbers of endospores in deep warm  
50 strata, with depth profiles revealing that temperature influences sporulation and germination<sup>13</sup>.  
51 This is consistent with the prevalence of endospore forming *Firmicutes* in microbiome surveys of  
52 hot oil reservoirs from around the world<sup>15</sup> where they actively contribute to biogeochemical  
53 cycling. In the energy limited deep biosphere, these petroleum systems represent energy rich

54 oases<sup>16,17</sup> that select for thermophilic organotrophy. Accordingly, cell densities in oil reservoirs  
55 can be an order of magnitude higher than those in surrounding sediments at the same depth<sup>18</sup>.

56  
57 Hydrocarbon seepage up and out of deep petroleum systems is widespread in the ocean<sup>19</sup>. Studies  
58 of thermophilic spores in cold surface sediments globally<sup>20,21</sup> have invoked warm-to-cold dispersal  
59 routes like hydrocarbon seeps to explain these observations<sup>22</sup>. In the Gulf of Mexico where cold  
60 seeps are common<sup>23</sup>, spore-forming thermophiles are correlated with the presence of migrated  
61 liquid hydrocarbons<sup>24</sup> and buoyant gas migration mediates upward microbial dispersal in the top  
62 few centimeters<sup>25</sup>. Whether viable cells from deeper and hotter subsurface layers can be similarly  
63 circulated over greater depths and timescales by seepage and subsequent burial remains  
64 hypothetical. Here we compare deep-sea sediments from the NW Atlantic Ocean (Extended Data  
65 Fig. 1) using geophysics, hydrocarbon geochemistry, spore germination dynamics and genomics  
66 to demonstrate the dispersal cycle of viable cells throughout the marine subsurface. This  
67 geologically mediated microbial loop transports living biomass via upward seepage and downward  
68 burial and represents a previously overlooked mechanism for ecological maintenance and  
69 preservation of life in the energy limited subsurface biosphere.

70  
71 Structural geology indicative of deep subsurface to surface geofluid conduits was determined by  
72 multichannel 2D and 3D seismic reflection surveys along the NW Atlantic Scotian Slope.  
73 Geophysical surveys covered ~70,000 km<sup>2</sup> and obtained ~10,000 m of subsurface stratigraphic  
74 imagery in up to 3,400 m water depth (Fig. 1a). Seabed seep detection in deep-sea settings like  
75 this is very challenging<sup>26</sup>, thus a multi-disciplinary strategy was employed. Co-location at the  
76 seabed of the up-dip limit of deep-seated faults and seismic reflection anomalies considered to be

77 direct hydrocarbon indicators were used to identify potential subsurface seep networks<sup>27</sup> (Fig. 1b).  
78 These large-scale geophysical survey results were refined through high-resolution seismic  
79 reflection, side-scan sonar and multibeam bathymetry. Morphological features included a  
80 mounded structure with high backscatter intensity intersected by an elongated fracture-like  
81 depression (Fig. 1c) and a circular pockmark, suggesting the presence of a seep-like structure.  
82 Immediately beneath these features, high-resolution subsurface seismic profiling revealed a  
83 localized acoustic blanking zone (Fig. 1d) suggesting the presence of gas<sup>28</sup> and a hydrocarbon  
84 migration pathway through subsurface sediments.

85  
86 Locations showing seismic evidence of migrated hydrocarbons originating from a deep subsurface  
87 source (Supplementary Table 1) were examined in greater detail by comparing hydrocarbon  
88 signals from 14 different sites that were sampled by piston coring (Fig. 2a; Supplementary Table  
89 2). Higher concentrations of thermogenic C<sub>2</sub>–nC<sub>4</sub> compounds and heavy δ<sup>13</sup>C values for methane  
90 (-42 to -52‰) in interstitial gas, coupled with liquid hydrocarbon extracts featuring elevated  
91 nC<sub>17</sub>/nC<sub>27</sub> ratios and a lack of odd-over-even alkane distributions in the nC<sub>23–33</sub> range, provided  
92 clear evidence of migrated hydrocarbons at two sites. This was confirmed by higher proportions  
93 of thermally derived diasteranes relative to regular steranes (% 27 dβ S) and more thermally mature  
94 terpane distributions (C<sub>30</sub> αβ relative to C<sub>31</sub> αβ 22R hopane) in these cores. At the 12 other sites,  
95 thermogenic hydrocarbon signals were either inconclusive (n=4) or not detected (n=8).

96  
97 To compare thermophilic spore-forming bacterial populations in cores with and without evidence  
98 of thermogenic hydrocarbons, endospore germination and thermophile enrichment was stimulated  
99 in high temperature anoxic incubations (40–60°C following pasteurization at 80°C; Extended Data

100 Fig. 3). Assessing microbial community composition by 16S rRNA gene profiling of incubated  
101 surface sediments from all 14 locations showed divergent profiles for hydrocarbon-positive  
102 locations (Fig. 2b; Supplementary Table 3). Statistical comparisons revealed 42 unique amplicon  
103 sequence variants (ASVs), all belonging to spore-forming bacterial taxa, correlated with upward  
104 seepage of thermogenic hydrocarbons (IndicSpecies,  $P < 0.05$ ; Supplementary Table 5). Putative  
105 fermentative organotrophs such as *Paramaledivibacter* and *Caminicella*, as well as sulfate-  
106 reducing *Desulfotomaculales* and *Candidatus* Desulforudis, showed strong hydrocarbon  
107 association (Fig. 3a). None of these groups were detected by applying the same DNA sequencing  
108 method to unincubated sediment (Supplementary Table 3), likely owing both to their low relative  
109 abundance *in situ*<sup>29</sup> and their multi-layered endospore coat not yielding to standard cell lysis  
110 protocols for DNA extraction<sup>30</sup>.

111  
112 To assess the prevalence of these bacteria in deep petroleum systems, we curated a dataset of 16S  
113 rRNA gene sequences from 59 different oil reservoir microbiomes from around the world  
114 (Supplementary Table 6). Seep-associated thermophilic endospore lineages identified in cold  
115 deep-sea sediments analysed here are found in high proportions in subsurface petroleum systems,  
116 especially *Caminicellaceae* and *Desulfotomaculales* which each make up 2–3% of the global oil  
117 reservoir microbiome dataset (Fig. 3b). ASV assessment at finer taxonomic resolution confirms  
118 close genetic relatedness between thermophilic endospores in Scotian Slope sediments and  
119 bacteria found in different subsurface oil reservoirs (Fig. 3c; Extended Data Fig. 4). Genomes of  
120 these dormant spores encode the potential for anaerobic hydrocarbon biodegradation, favouring  
121 their selection and growth in deep petroleum-bearing sediments (Fig. 3d). Metagenome-assembled  
122 genomes (MAGs) of *Caminicella*, *Paramaledivibacter*, *Desulfohalotomaculum* and *Bacillus* with

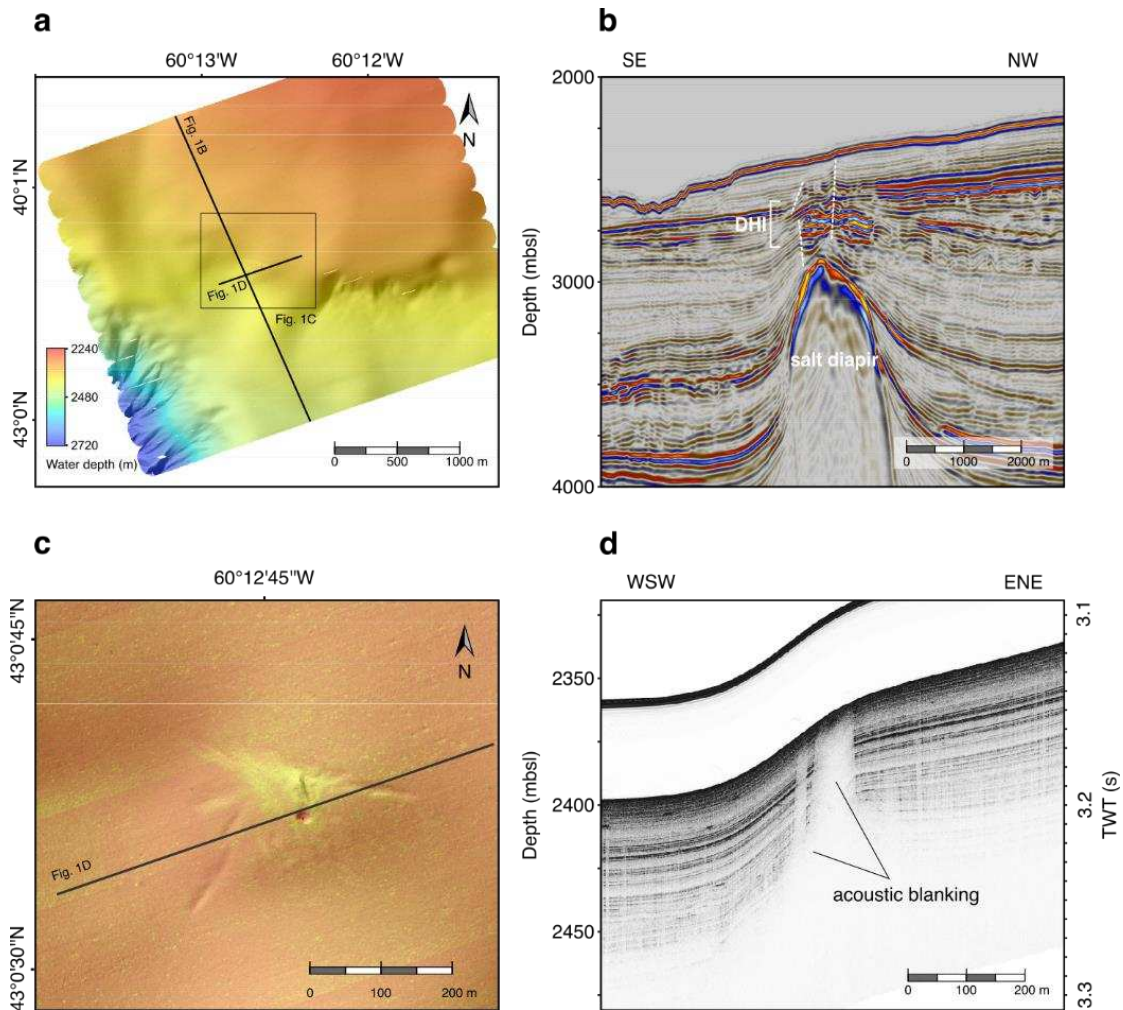
123 rRNA sequences matching the indicator ASVs (Fig. 3; Supplementary Table 7) contain glycyl-  
124 radical enzymes proposed to mediate anaerobic alkane biodegradation via addition to fumarate<sup>31,32</sup>.  
125 Based on newly developed Hidden Markov Models for annotating alkylsuccinate synthases<sup>33</sup>,  
126 putative *assA* gene sequences in thermophilic spores diverge from canonical *assA* found in  
127 mesophilic *Proteobacteria* (Extended Data Fig. 5). This divergent clade includes thermophiles  
128 from hot oil reservoirs such as <sup>U</sup>*Petromonas tenebris*<sup>34</sup> and *Archaeoglobus fulgidus*<sup>35</sup>. Cold  
129 sediment MAGs also contain sporulation genes (Fig. 3d) including the *spo0A* master  
130 transcriptional response regulator<sup>36</sup> as well as genes for synthesizing α/β-type small acid-soluble  
131 proteins (e.g., *sspD*) and dipicolinic acid (e.g., *dpaB*) involved in DNA protection<sup>37</sup> (for a full list  
132 of sporulation genes see Supplementary Table 9).

133

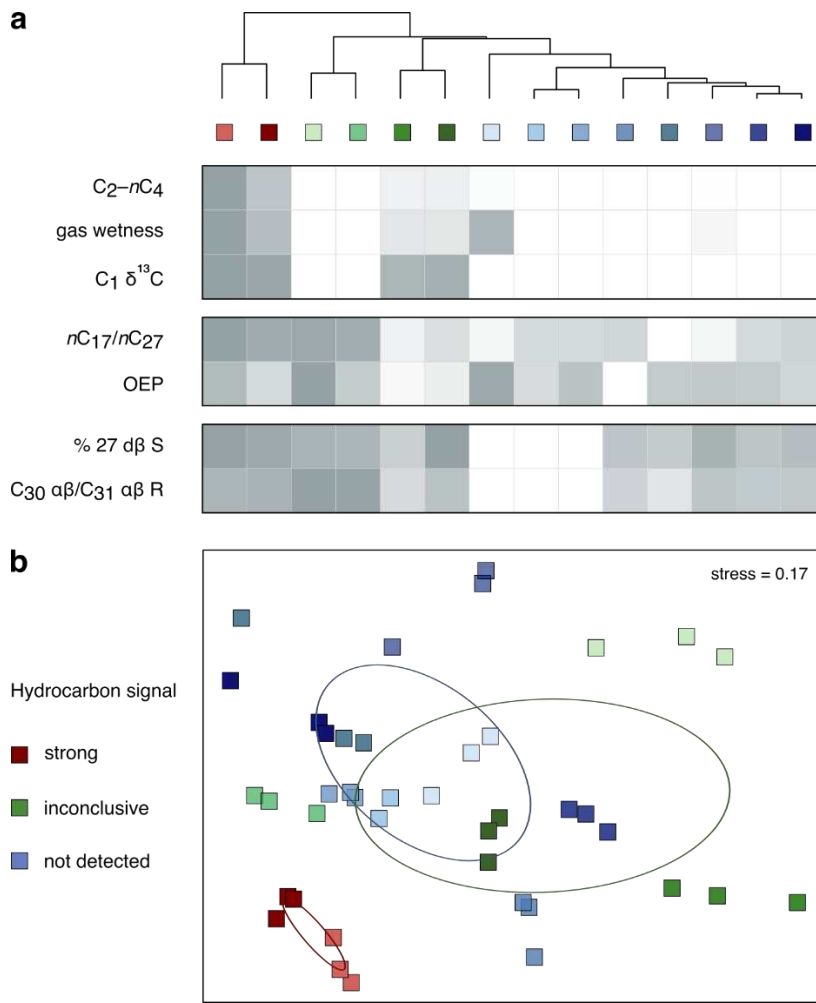
134 Maintenance of dormancy has been proposed as a necessary pre-requisite for microbial taxa to  
135 exhibit biogeographic patterns over large distances and timescales<sup>12</sup>. Thermophilic endospores  
136 originating from deep petroleum-bearing sediments exemplify large-scale biogeography by  
137 connecting anaerobic hydrocarbon biodegradation and other microbial activities in the subsurface  
138 with intervening periods of large-scale migration in a dormant, sporulated state. Recurrent cyclical  
139 dispersal facilitates this scenario, consistent with a framework for microbial biogeography that  
140 features the same environment being both the origin and eventual destination for migrating  
141 populations<sup>12</sup>. Upon being transported out of the subsurface and into the benthos (Fig. 4a), further  
142 transport of spores via bottom water currents precedes eventual re-entry into the seabed (Fig. 4b).  
143 In the cold surface sediment of the Scotian Slope, thermophilic spores were detected in all of the  
144 cores that were collected, including those lacking geochemical evidence of hydrocarbon seepage  
145 (Supplementary Table 3). Dipicolinic acid concentrations within the top few metres demonstrate

146 constant deposition and burial of endospores (Fig. 4c), with numbers in this region similar to or  
147 exceeding the seabed global average<sup>2</sup>. High temperature anoxic incubation of sediment from these  
148 depths to germinate thermophilic spores shows that they remain viable during burial (Extended  
149 Data Fig. 6). In sediments that eventually become petroleum systems at even greater depths where  
150 these temperatures occur naturally, the activation of these dormant bacteria by suitable nutrients  
151 and heat completes a subsurface microbial loop of viable cells circulating out of and back into the  
152 deep biosphere (Fig. 4).

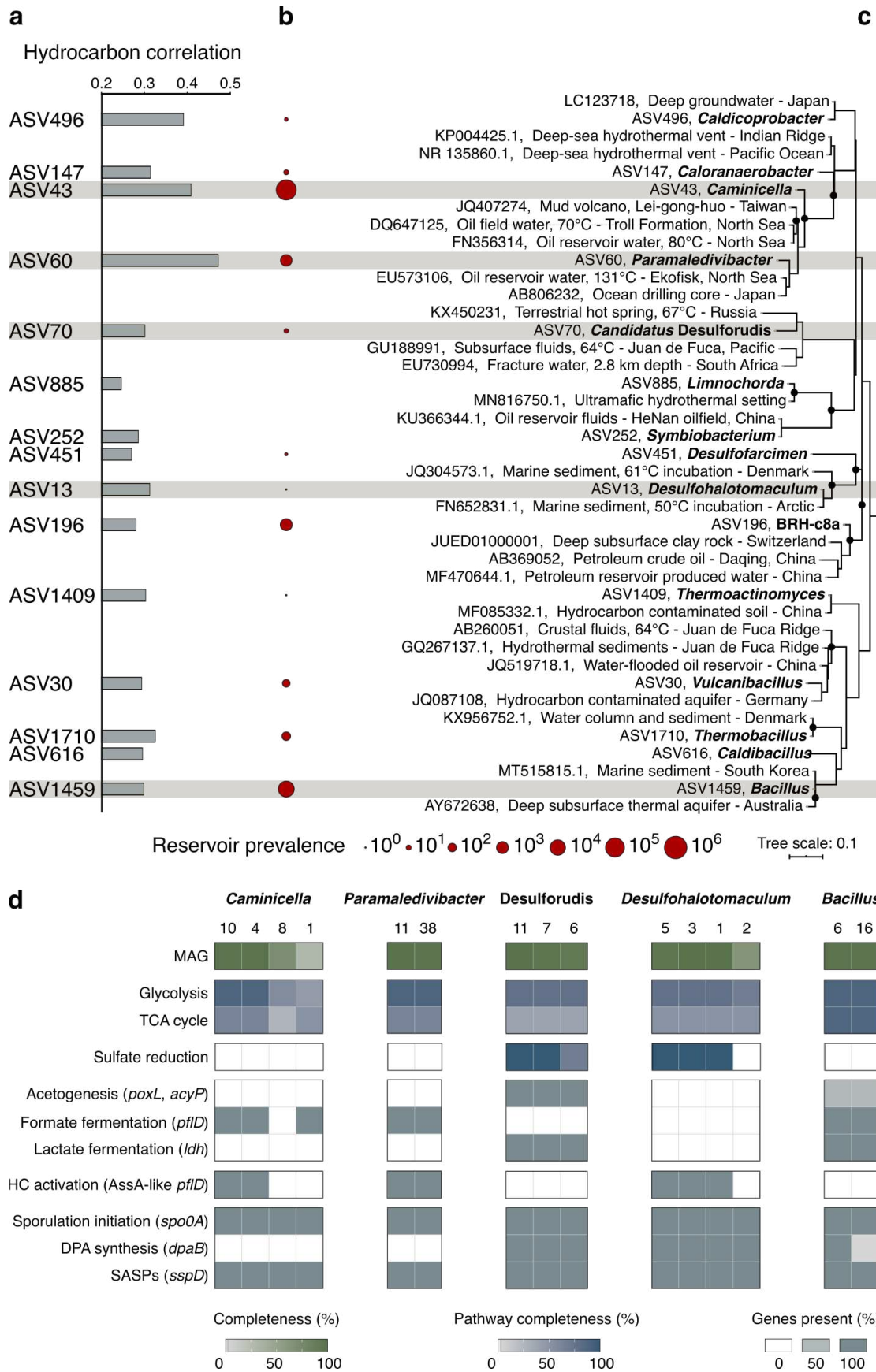
153  
154 Subsurface marine sediments contain 12–45% of Earth’s microbial biomass and are central to the  
155 planet’s biogeochemical cycling<sup>40</sup>. This is especially true in petroleum systems that control and  
156 are controlled by subsurface microbial populations<sup>31,41</sup>. Despite the importance of these processes,  
157 research on the subsurface microbiome rarely focuses on ecological factors like dispersal and  
158 selection, preventing a more complete understanding of deep biosphere ecosystems<sup>4</sup>. The results  
159 presented here demonstrate that geological processes of geofluid flow and sedimentation connect  
160 deep petroleum systems with the ocean and mediate a recurrent and spatially extensive cycle of  
161 microbial dispersal throughout the subsurface. This circulation of living biomass is uniquely  
162 characterized by defined episodes of microbial activity in petroleum-bearing sediments  
163 interspersed by long intervals of passive dispersal — an ecological sequence that is difficult to  
164 delineate as clearly in other environmental settings<sup>8</sup>. By connecting the physical and physiological  
165 factors that govern survival and evolution in the deep biosphere, this subsurface microbial loop  
166 showcases the geosphere as a model system for understanding the interplay between microbial  
167 dispersal and selection in the biosphere at large spatial and temporal scales.



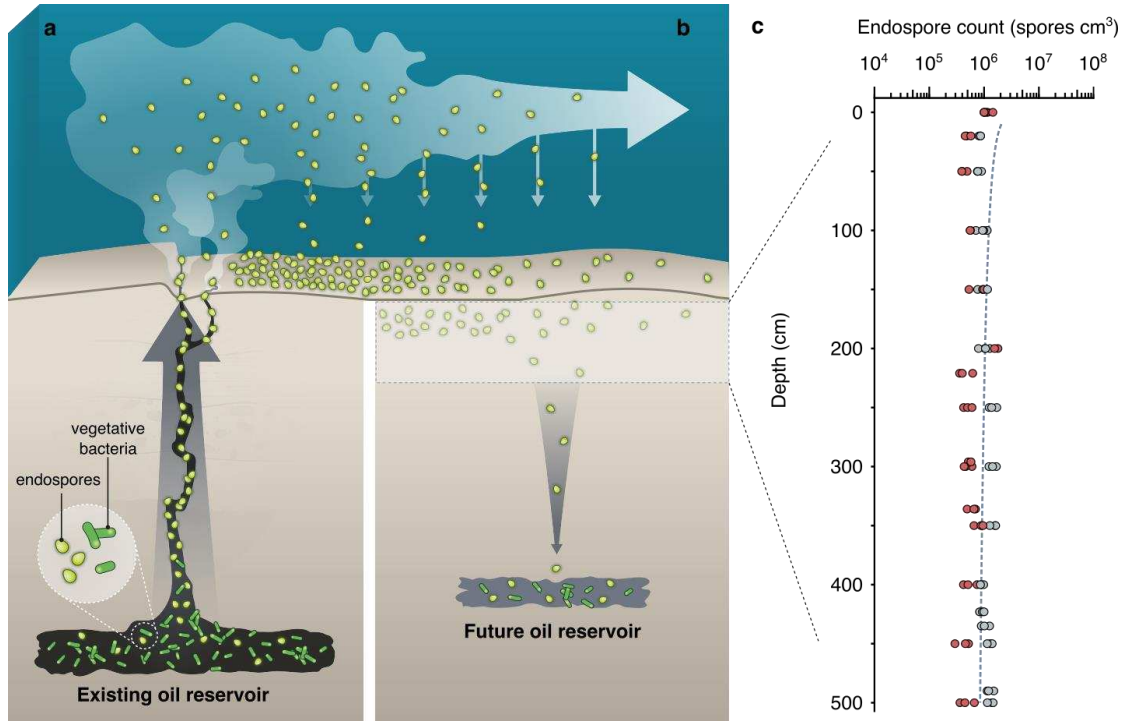
169 **Fig. 1. Deep subsurface to surface geofluid migration.** **a**, Seafloor surface map derived from  
170 AUV-based multibeam bathymetric sonar data at one location. **b**, 3D seismic cross section  
171 showing a buried salt diapir, the location and direction of crestal faults (white dashed lines), and  
172 an interval with direct hydrocarbon indicators (DHI). **c**, Combined mosaic of side-scan sonar data  
173 and shaded relief bathymetry of the area surrounding a seep structure, indicating a pockmark  
174 feature as well as a small mound morphology. High backscatter intensity, related to distinctive  
175 properties of near-surface sediment, is shown in light-yellowish tones. **d**, AUV-based sub-bottom  
176 profiling showing localized acoustic blanking under the seep structure, indicative of upward fluid  
177 migration.



179 **Fig. 2. Hydrocarbon geochemistry and microbial community variance between seabed**  
180 **sampling sites. a**, Gas ( $\sum C_2-nC_4$ , gas wetness, and  $C_1 \delta^{13}C$ ), liquid hydrocarbon extract  
181 ( $nC_{17}/nC_{27}$  and odd-over-even predominance) and biomarker (% 27 d $\beta$  S and  $C_{30} \alpha\beta/C_{31} \alpha\beta$  22R)  
182 measurements to assess the presence of thermogenic hydrocarbons. Each parameter is scaled  
183 between 0 and 1 as shown in the heatmap. Cores are represented by average values in instances  
184 where multiple depths from a core were tested (values provided in Supplementary Table 2).  
185 Hierarchical clustering highlights groups of sites where the evidence for the presence of  
186 thermogenic hydrocarbons is strong (red), inconclusive (green) or not detected (blue). **b**, Bray-  
187 Curtis dissimilarity in microbial community composition after sediment incubation at 50°C  
188 reflected the three geochemical groupings (ellipses indicate standard deviations of weighted  
189 averaged means of within-group distances for each of the three groups; see Extended Data Fig. 2  
190 for plots from 40 and 60°C incubations). Sites with strong thermogenic hydrocarbon signals have  
191 distinct microbial populations after high temperature incubation (Supplementary Table 4).



193 **Fig. 3. Oil reservoir provenance of seep-associated thermophiles.** **a**, Correlation of  
194 thermophilic spore-forming bacterial amplicon sequence variants (ASVs) with thermogenic  
195 hydrocarbons. Highest ranking ASVs from each of 15 different genera are shown (representing 42  
196 hydrocarbon-correlated ASVs in total). **b**, Prevalence of these genera in 59 oil reservoir  
197 microbiome assessments (11 million 16S rRNA gene sequences in total). **c**, Maximum likelihood  
198 phylogeny showing the 15 representative hydrocarbon-correlated ASVs and close relatives in the  
199 GenBank database (for all 42 indicator ASVs see Fig. S3). Black circles at the branch nodes  
200 indicate >80% bootstrap support (1,000 re-samplings), and the scale bar indicates 10% sequence  
201 divergence as inferred from PhyML. **d**, Metagenome-assembled genomes (MAGs) matching  
202 ASVs of interest (see corresponding brown shading in **a–c**) were assessed for anaerobic alkane  
203 degradation, sporulation and other metabolic features (see Supplementary Table 8 for pathway  
204 definitions).



205

**Fig. 4. Subsurface microbial loop mediated by seepage, sedimentation, dormancy and environmental selection.** a, Endospore-forming microbial populations actively inhabiting deep petroleum systems get dispersed upwards as dormant spores by hydrocarbon seepage along geological conduits. Endospores entering the deep-sea are dispersed laterally by bottom water currents. b, Endospores get deposited on the seabed and undergo burial. c, Endospore burial is revealed by triplicate measurements of dipicolinic acid concentrations in the upper few metres of the seabed in two Scotian Slope sediment cores where hydrocarbons were not detected. The dashed regression line reflects the global average estimated for endospores in the marine subseafloor biosphere<sup>2</sup>. Survival of some fraction of these endospores over long time-scales<sup>10,38</sup> enables environmental selection (i.e., germination and activity) by suitable substrates and heat-favorable conditions that establish in sediments where oil migrates into to establish a reservoir<sup>39</sup>. The sequence shown in a and b completes a ‘subsurface microbial loop’ that incorporates cell dispersal and biogeochemical cycling in Earth’s deep biosphere.

219

220 **Main references**

221 1. Bar-On, Y. M., Phillips, R. & Milo, R. The biomass distribution on Earth. *Proc. Natl. Acad. Sci.* **115**, 6506–6511 (2018).

223 2. Wörmer, L. et al. Microbial dormancy in the marine subsurface: Global endospore abundance  
224 and response to burial. *Sci. Adv.* **5**, (2019).

225 3. Hoehler, T. M. & Jørgensen, B. B. Microbial life under extreme energy limitation. *Nat. Rev. Microbiol.* **11**, 83–94 (2013).

227 4. Biddle, J. F. et al. Prospects for the study of evolution in the deep biosphere. *Front. Microbiol.* **2**, 285 (2012).

229 5. Darwin, C. On the origin of species by means of natural selection, or preservation of favoured  
230 races in the struggle for life. London: J. Murray, 1859.

231 6. Baas Becking, L. G. M. Geobiologie of Inleiding Tot de Milieukunde (W. P. Van Stockum &  
232 Zoon, The Hague, Netherlands, 1934).

233 7. Hanson, C. A., Fuhrman, J. A., Horner-Devine, M. C. & Martiny, J. B. H. Beyond  
234 biogeographic patterns: processes shaping the microbial landscape. *Nat. Rev. Microbiol.* **10**,  
235 497–506 (2012).

236 8. Ward, B. A., Cael, B. B., Collins, S. & Young, C. R. Selective constraints on global plankton  
237 dispersal. *Proc. Natl. Acad. Sci.* **118**, (2021).

238 9. Setlow, B., Atluri, S., Kitchel, R., Koziol-Dube, K. & Setlow, P. Role of dipicolinic acid in  
239 resistance and stability of spores of *Bacillus subtilis* with or without DNA-protective  $\alpha/\beta$ -type  
240 small acid-soluble proteins. *J Bacteriol.* **188**, 3740–3747 (2006).

241 10. Fang, J. et al. Predominance of viable spore-forming piezophilic bacteria in high-pressure  
242 enrichment cultures from ~1.5 to 2.4 km-deep coal-bearing sediments below the ocean floor.  
243 *Front. Microbiol.* **8**, 137 (2017).

244 11. Lennon, J. T. & Jones, S. E. Microbial seed banks: the ecological and evolutionary implications  
245 of dormancy. *Nat. Rev. Microbiol.* **9**, 119–130 (2011).

246 12. Mestre, M. & Höfer, J. The microbial conveyor belt: Connecting the globe through dispersion  
247 and dormancy. *Trends Microbiol.* (2020).

248 13. Heuer, V. B. et al. Temperature limits to deep subseafloor life in the Nankai Trough subduction  
249 zone. *Science* **370**, 1230–1234 (2020).

250 14. Lomstein, B. A., Langerhuus, A. T., D’Hondt, S., Jørgensen, B. B. & Spivack, A. J. Endospore  
251 abundance, microbial growth and necromass turnover in deep sub-seafloor sediment. *Nature*  
252 **484**, 101–104 (2012).

253 15. Hubert, C. R. et al. Massive dominance of Epsilonproteobacteria in formation waters from a  
254 Canadian oil sands reservoir containing severely biodegraded oil. *Environ. Microbiol.* **14** 387–  
255 404 (2012).

256 16. Orphan, V. J., Taylor, L. T., Hafenbradl, D. & Delong, E. F. Culture-dependent and culture  
257 independent characterization of microbial assemblages associated with high-temperature  
258 petroleum reservoirs. *Appl. Environ. Microbiol.* **66**, 700–711 (2001).

259 17. Vigneron, A. et al. Succession in the petroleum reservoir microbiome through and oil field  
260 production lifecycle. *ISME J.* **11**, 2141–2154 (2017).

261 18. Bennett, B. et al. The controls on the composition of biodegraded oils in the deep subsurface  
262 – Part 3. The impact of microorganism distribution on petroleum geochemical gradients in  
263 biodegraded petroleum reservoirs. *Org. Geochem.* **56**, 94–105 (2013).

264 19. Judd, A. G. The global importance and context of methane escape from the seabed. *Geo-Mar.*  
265 *Lett.* **23**, 147–154 (2003).

266 20. Müller, A. L. et al. Endospores of thermophilic bacteria as tracers of microbial dispersal by  
267 ocean currents. *ISME J.* **8**, 1153–1165 (2014).

268 21. Hanson, C. A. et al. Historical factors associated with past environments influence the  
269 biogeography of thermophilic endospores in Arctic marine sediments. *Front Microbiol.* **10**, 1–  
270 14 (2019).

271 22. Hubert, C. et al. A constant flux of diverse thermophilic bacteria into the cold Arctic seabed.  
272 *Science* **325**, 1541–1544 (2009).

273 23. MacDonald, I. R. Natural and unnatural oil slicks in the Gulf of Mexico. *J. Geophys. Res.*  
274 *Oceans* **120**, 8364–8380 (2015).

275 24. Chakraborty, A. et al. Thermophilic endospores associated with migrated thermogenic  
276 hydrocarbons in deep Gulf of Mexico marine sediments. *ISME J.* **12**, 1895–1906 (2018).

277 25. Chakraborty, A. et al. Hydrocarbon seepage in the deep seabed links subsurface and seafloor  
278 biospheres. *Proc. Natl. Acad. Sci.* **117**, 11029–11037 (2020).

279 26. Abrams, M. A. Marine seepage variability and its impact on evaluating the surface migrated  
280 hydrocarbon seep signal. *Mar. Pet. Geol.* **121** (2020).

281 27. Nanda, N. C. Direct Hydrocarbon Indicators (DHI) in *Seismic data interpretation and*  
282 *evaluation for hydrocarbon exploration and production*. N. C. Nanda (Springer, Switzerland,  
283 2016), pp. 103–113.

284 28. Judd, A. G. & Hovland, M. Seabed Fluid Flow: The Impact on Geology, Biology and the  
285 Marine Environment. Cambridge University Press, Cambridge, 163–178 (2007).

286 29. de Rezende, J. R., Hubert, C. R. J., Røy, H., Kjeldsen, K. U. & Jørgensen, B. B. Estimating the  
287 abundance of endospores of sulfate-reducing bacteria in environmental samples by inducing  
288 germination and exponential growth. *Geomicrobiol. J.* **4**, 338–345 (2017).

289 30. Wunderlin, T., Junier, T., Roussel-Delif, L., Jeanneret, N. & Junier, P. Endospore-enriched  
290 sequencing approach reveals unprecedented diversity of Firmicutes in sediments. *Environ.*  
291 *Microbiol. Rep.* **6**, 631–639 (2014).

292 31. Jones, D. M. et al. Crude-oil biodegradation via methanogenesis in subsurface petroleum  
293 reservoirs. *Nature* **451**, 176–180 (2008).

294 32. Gray, N. D. et al. Biogenic methane production in formation waters from a large gas field in  
295 the North Sea. *Extremophiles* **13**, 511–519 (2009).

296 33. Khot, V. et al. CANT-HYD: A curated database of phylogeny-derived Hidden Markov Models  
297 for annotation of marker genes involved in hydrocarbon degradation. bioRxiv.  
298 <https://www.biorxiv.org/content/10.1101/2021.06.10.447808v1>

299 34. Christman, G. D., León-Zayas, R. I., Zhao, R., Summers, Z. M. & Biddle, J. F. Novel clostridial  
300 lineages recovered from metagenomes of a hot oil reservoir. *Sci. Rep.* **10**, 8048 (2020).

301 35. Khelifi, N. et al. Anaerobic oxidation of long-chain n-alkanes by the hyperthermophilic sulfate-  
302 reducing archaeon, *Archaeoglobus fulgidus*. *ISME J.* **8**, 2153–2166 (2014).

303 36. Hoch, J. A. Regulation of the phosphorelay and the initiation of sporulation in *Bacillus subtilis*.  
304 *Annu. Rev. Microbiol.* **47**, 441–465 (1993).

305 37. Setlow, B., Atluri, S., Kitchel, R., Koziol-Dube, K. & Setlow, P. Role of dipicolinic acid in  
306 resistance and stability of spores of *Bacillus subtilis* with or without DNA-protective  $\alpha/\beta$ -type  
307 small acid-soluble proteins. *J Bacteriol.* **188**, 3740–3747 (2006).

308 38. de Rezende, J. R. et al. Dispersal of thermophilic *Desulfotomaculum* endospores into Baltic  
309 Sea sediments over thousands of years. *ISME J.* **7**, 72–84 (2013).

310 39. Magoon, L. B. & Dow, W. G. The Petroleum System — From Source to Trap (Am. Assoc.  
311 Petroleum Geologists, Tulsa, Mem. 60, 1994).

312 40. Morono, Y. et al. Aerobic microbial life persists in oxic marine sediment as old as 101.5 million  
313 years. *Nat. Commun.* **11** (2020).

314 41. Wilhelms, A. et al. Biodegradation of oil in uplifted basins prevented by deep-burial  
315 sterilization. *Nature* **411**, 1034–1037 (2001).

316 **Methods**

317 **Seismic data acquisition and processing**

318 Multiple two- and three-dimensional multi-channel seismic surveys performed here for the  
319 identification of seafloor seeps relied on an earlier regional 28,000 km<sup>2</sup> 2D seismic survey. The  
320 earlier survey was shot in a 6 km grid, acquiring 14 seconds of data with 80–106-fold and a 2  
321 millisecond sampling interval. The 1998 vintage used was processed to pre-stack time migrated  
322 data. 2D seismic survey interpretations were refined using the Shelburne 3D Wide Azimuth  
323 Seismic survey. This survey was acquired over 12,000 km<sup>2</sup> in the deep-water Shelburne sub-basin  
324 at 6.25 x 50 m bin spacing with a fold of 100. This vintage of data utilized both full 3D Anisotropic  
325 Kirchhoff pre-stack time migration (PSTM) and full volume anisotropic Kirchhoff pre-stack depth  
326 migration (PSDM) with vertical transverse isotropy. PSTM had a processed bin size of 12.5 x 25  
327 m, while PSDM had an output bin size of 25 x 25 m. Data were interpreted using the Petrel E&P  
328 Software Platform (Schlumberger Limited).

329

330 High-resolution seismic reflection profiles (data not shown) were used to investigate the  
331 subsurface stratigraphy in the vicinity of seep prospects to inform autonomous underwater vehicle  
332 (AUV) survey and coring locations. Profiles were collected during three expeditions between 2015  
333 and 2018 onboard the CCGS *Hudson*<sup>42–44</sup> using a Huntec single-channel Deep Tow Seismic (DTS)  
334 sparker system. Tow depth was ~100 m beneath the sea surface with the source fired at a moving  
335 time interval between 1 and 3 seconds. The peak frequency for the Huntec DTS sparker is  
336 approximately 1,500 Hz and spans from 500–2,500 Hz. Raw sparker data was processed using the  
337 VISTA Desktop Seismic Data Processing Software (Schlumberger Limited) and included Ormsby  
338 band-pass filtering, scaling correction, automatic gain control and trace mixing.

339

340 An autonomous underwater vehicle (AUV) was deployed from the vessel *Pacific Constructor* to  
341 collect high-resolution geophysical data over a 2.5 x 2.5 km area at the location of cores 16-41 and  
342 18-7 in August 2020. The HUGIN 6000 AUV (Kongsberg Maritime) was steered approximately  
343 40 m above the seafloor for multibeam bathymetric, side-scan sonar and sub-bottom profiling data  
344 collection using a Kongsberg EM 2040 multibeam echosounder and a EdgeTech 2205 sonar  
345 system, respectively. EM2040 Multibeam bathymetric data was acquired at a frequency of 400  
346 kHz, with a continuous waveform (CW) pulse and synchronized with Doppler velocity log.  
347 Multibeam bathymetric data was processed using Caris and Eiva suite. Side Scan Sonar data was  
348 acquired at a frequency of 230 kHz and post-processing of the data was completed in Sonarwiz.  
349 The sub-bottom profiler was operated over the frequency range of 1–9 kHz with a 20-millisecond  
350 pulse. The high-resolution seismic data was integrated and analyzed using IHS Kingdom Suite  
351 (IHS Markit Ltd). Acoustic travel times for high resolution sub-bottom profiler lines were  
352 converted into depths by using an average seismic velocity of 1,500 m.s<sup>-1</sup>.

353

### 354 **Marine sediment sampling**

355 Seabed surface sediments in 2,000 to 3,400 m water depth were collected by piston and gravity  
356 coring from different locations on the Scotian Slope, offshore Nova Scotia, Canada (Fig. 1;  
357 Supplementary Table 1) during May-June expeditions aboard the CCGS *Hudson* in 2015, 2016  
358 and 2018<sup>42–44</sup>. Piston cores, trigger weight cores (smaller cores that release the head weight of the  
359 piston core) and gravity cores ranged from 0.18 to 8.34 m in length. Upon recovery, cores were  
360 split longitudinally onboard the ship. Sediment intervals from the base of the core (5-10 cm) were  
361 transferred to gas-tight IsoJars® (Isotech Laboratories Inc., USA), immediately flushed with

362 nitrogen, and stored at -20°C prior to interstitial gas analysis. Similar intervals from variable depths  
363 along the cores, selected based on indications of visible hydrocarbon staining or odour,  
364 fluorescence, or sandy lithology, were stored in aluminum foil at -20°C for eventual hydrocarbon  
365 analysis, and in sterile Whirl-Pak® bags or glass jars at 4°C for eventual high temperature  
366 endospore germination experiments. Sediment intervals at the top of the core (either 0–10 or 0–20  
367 cm below seabed) were similarly transferred to sterile Whirl-Pak® bags or sterile glass jars.

368

### 369 **Hydrocarbon geochemical analysis**

370 Interstitial gas analysis was performed on aliquots of IsoJar® (Isotech Laboratories Inc., USA)  
371 headspace transferred into Exetainers® (Labco Limited, UK). Sample volumes of 1 mL were  
372 injected into an Agilent 7890 RGA Gas Chromatograph (Agilent Technologies, USA). A flame  
373 ionisation detector determined C<sub>1</sub>–C<sub>5</sub> hydrocarbon gas concentrations that were used to calculate  
374 gas wetness. Carbon isotopic composition ( $\delta^{13}\text{C}$ ) of hydrocarbon gas components was determined  
375 by gas chromatography combustion isotope ratio mass spectrometry; headspace aliquots were  
376 analyzed on a Trace 1310 Gas Chromatograph (Thermo Fisher Scientific, USA) interfaced to a  
377 Delta V Isotope Ratio Mass Spectrometer (Thermo Fisher Scientific, USA).

378

379 Sediments were analyzed for hydrocarbon biomarkers in subsamples where sufficient extract  
380 yields were recovered. Accordingly, no extract yield, or insufficient yields to determine biomarker  
381 concentrations, were considered indicative of the absence of hydrocarbon seepage. Organic matter  
382 was extracted from sediment by adding dichloromethane with 7% (v/v) methanol, mixing the  
383 solution in an ultrasonic bath for 15 min and then leaving at room temperature for 24 h. Extractable  
384 organic matter (EOM) was evaporated to dryness and weighed. Asphaltenes were removed by

385 pentane addition in excess (40 times the volume of EOM), storage for 12 h, and centrifugation.  
386 Gas chromatography analysis of the EOM was performed on an Agilent 7890A Gas  
387 Chromatograph (Agilent Technologies, USA). Saturate and aromatic hydrocarbon fractions  
388 showing possible evidence of thermogenic hydrocarbons were analyzed further using a Micromass  
389 ProSpec Gas Chromatography-Mass Spectrometer (Waters Corporation, USA). Geochemical  
390 analyses were performed by Applied Petroleum Technology, Norway, to the standards used in  
391 industrial hydrocarbon assessments. Geochemistry data was collectively interpreted for evidence  
392 of thermogenic hydrocarbons likely derived from subsurface hydrocarbon seeps. Hierarchical  
393 clustering (complete linkage clustering based on Euclidean distance) of geochemical  
394 measurements scaled between 0 and 1 over the range of values (0 representing weakest  
395 thermogenic signal and 1 representing the strongest thermogenic signal) was used to further assess  
396 and visualise groups of sites with similar geochemical signatures (Fig. 2a).

397

### 398 **Sediment incubation at elevated temperatures**

399 Sediments were investigated for the germination and growth of dormant bacterial endospores.  
400 Following homogenizing by stirring within the sample container, up to 100 g of sediment was  
401 transferred into separate 250 mL serum bottles that were sealed with butyl rubber stoppers  
402 (Chemglass Life Sciences, Canada) and the headspace exchanged with N<sub>2</sub>:CO<sub>2</sub> (90:10%).  
403 Sediment slurries were prepared in a 1:2 (w/w) ratio with sterile, anoxic, synthetic seawater  
404 medium<sup>45</sup> containing 20 mM sulfate and amended with acetate, butyrate, formate, lactate,  
405 propionate, and succinate (5 mM each for surface sediments and 1 mM each for deeper sediments).  
406 Master sediment slurries were subdivided into replicate, sterile, anoxic 50 mL serum bottles sealed  
407 with butyl rubber stoppers. Slurries were pasteurized at 80°C for 1.5 h to kill vegetative cells and

408 select for heat-resistant endospores. Triplicate pasteurized slurries were immediately incubated at  
409 40, 50 or 60°C for up to 56 days to promote germination and growth of thermophilic endospore-  
410 forming bacteria. Subsamples (2 mL) were periodically removed using sterile N<sub>2</sub>:CO<sub>2</sub>-flushed  
411 syringes and stored at -20°C for molecular analysis.

412

#### 413 **16S rRNA gene amplicon sequencing**

414 Genomic DNA was extracted from triplicate slurries subsampled immediately before incubation  
415 (i.e., post-pasteurization), and periodically during the incubation, using the DNeasy PowerLyzer  
416 PowerSoil Kit (Qiagen, USA). Extractions were performed on 300 µL of slurry according to the  
417 manufacturer's protocol, except for inclusion of a 10 min incubation at 70°C immediately after the  
418 addition of Solution C1 to enhance cell lysis. Extraction blanks (Milli-Q water) were processed in  
419 parallel. DNA was quantified using the Qubit dsDNA High Sensitivity assay kit on a Qubit 2.0  
420 fluorometer (Thermo Fisher Scientific, Canada). The V3 and V4 hypervariable regions of the 16S  
421 rRNA gene were amplified in triplicate PCR reactions per extraction using the primer pair SD-  
422 Bact-341-bS17/SD-Bact-785-aA21<sup>46</sup> modified with Illumina MiSeq overhang adapters. All PCR  
423 reactions were performed in triplicate. All DNA extraction blanks and PCR reagent blanks were  
424 confirmed for negative amplification using agarose gel electrophoresis. Triplicate PCR products  
425 were pooled, purified using a NucleoMag NGS Clean-up and Size Select kit (Macherey-Nagel  
426 Inc., USA) and indexed. Sizes of indexed amplicons were verified using the High Sensitivity DNA  
427 kit on an Agilent 2100 Bioanalyzer system (Agilent Technologies, Canada). Indexed amplicons  
428 were pooled in equimolar amounts and sequenced on an in-house Illumina MiSeq benchtop  
429 sequencer (Illumina Inc., USA) using Illumina's v3 600-cycle reagent kit to obtain 300 bp paired-  
430 end reads.

431

432 **16S rRNA gene amplicon sequence processing**

433 A total of 20,589,990 raw paired-end reads were generated across six separate MiSeq runs. Primers  
434 were trimmed using Cutadapt version 2.7<sup>47</sup> prior to amplicon sequence variant (ASV) inference  
435 using DADA2 version 1.16<sup>48</sup> in base R version 3.6.1<sup>49</sup>. Forward and reverse read pairs were  
436 trimmed to a run-specific length defined by a minimum quality score of 25. Read pairs were  
437 filtered allowing no ambiguous bases and requiring each read to have less than two expected errors,  
438 and PhiX sequences removed. Reads were dereplicated providing unique sequences with their  
439 corresponding abundance. Error rates were estimated from sequence composition and quality by  
440 applying a core denoising algorithm for each sequencing run to account for run-to-run variability.  
441 Unique ASVs were inferred independently from the forward and reverse reads of each sample,  
442 using the run-specific error rates, and then pairs were merged if they overlapped with no  
443 mismatches. Chimeras were identified and removed, then an additional length trimming step  
444 removed sequence variants shorter than 400 nucleotides and larger than 435 nucleotides. A total  
445 of 32,018 ASVs were resolved from 11,355,683 quality-controlled reads. Taxonomy was assigned  
446 using the Ribosomal Database Project's k-mer-based naïve Bayesian classifier with the DADA2-  
447 formatted Silva database version 138<sup>50</sup>. Reads were randomly subsampled without replacement to  
448 the smallest library size ( $n=4,635$ ) using the *phyloseq* R package<sup>51</sup> prior to comparative analysis.

449

450 **Metagenome sequencing**

451 Genomic DNA extracted from four separate sediment slurries after 56 days of incubation was used  
452 for metagenomic sequencing. Library preparation and sequencing was conducted at the Center for  
453 Health Genomics and Informatics in the Cumming School of Medicine, University of Calgary.

454 DNA was sheared using a Covaris S2 ultrasonicator (Covaris, USA), and fragment libraries  
455 prepared using a NEBNext Ultra II DNA Library Prep Kit for Illumina (New England BioLabs,  
456 USA). Metagenomic libraries were sequenced on the Illumina NovaSeq platform (Illumina Inc.,  
457 USA) using an S4 flow cell with Illumina 300 cycle (2 × 150 bp) V1.5 sequencing kit.

458

#### 459 **Metagenome sequence processing**

460 A total of 65,786,766 raw reads from four metagenomic libraries were quality-controlled by  
461 trimming technical sequences (primers and adapters) and low-quality additional bases, and  
462 filtering artifacts (phiX), low-quality reads and contaminated reads using BBduk (BBTools suite,  
463 <http://jgi.doe.gov/data-and-tools/bbtools>). Trimmed and filtered reads from each metagenome  
464 were assembled separately, as well as co-assembled, using MEGAHIT version 1.2.2<sup>52</sup> using  
465 default parameters and with <500 bp contigs removed. Binning of the four assemblies and one co-  
466 assembly was performed using MetaBAT 2 version 2.12.1<sup>53</sup>. Contamination and completeness of  
467 the resulting MAGs were estimated using CheckM version 1.0.11<sup>54</sup> with the lineage-specific  
468 workflow. Ribosomal rRNA genes were identified in unbinned reads using phyloFlash<sup>55</sup> and in  
469 binned reads using rRNAFinder implemented in MetaErg version 1.2.0<sup>56</sup>. Protein coding genes  
470 were predicted and annotated against curated protein sequence databases (Pfam, TIGRFAM, and  
471 Swiss-Prot) using MetaErg version 1.2.0<sup>56</sup>. Metabolic pathways were identified using KEGG  
472 Decoder<sup>57</sup> to parse genes annotated with KEGG Orthology using BlastKOALA<sup>58</sup>. Hydrocarbon  
473 degradation genes were additionally annotated using CANT-HYD<sup>33</sup> following gene predictions  
474 made using Prodigal version 2.6.3<sup>59</sup>. MAGs were classified with GTDB-Tk version 1.3.0<sup>60</sup> and by  
475 alignment with Silva database version 138<sup>50</sup> using mothur version 1.39.5<sup>61</sup> in instances where 16S  
476 rRNA gene was recovered by rRNAFinder<sup>56</sup>.

477

478 MAGs for the seep-associated taxa were identified by alignment of predicted 16S rRNA gene  
479 sequences recovered from bins with the seep indicator ASV sequences highlighted by IndicSpecies  
480 (see below). An alignment identity of 100% across the full length of the amplicon was required to  
481 confirm association. In instances where a V3-V4 overlapping 16S rRNA gene sequence was not  
482 recovered in the MAG, taxonomic classification of the partial 16S rRNA gene, the MAG (GTDB-  
483 Tk version 1.3.0<sup>60</sup>), or the sample by phyloFlash was used to identify possible associations to seep-  
484 associated taxa. If the most abundant ASV in an unrarefied 16S rRNA gene amplicon library, with  
485 the same taxonomic classification as the recovered 16S rRNA gene or MAG, corresponded to the  
486 most abundant ASV in that sample, a probabilistic association was assumed and the MAG was  
487 retained for further analysis. Replicate MAGs were identified from cluster groups based on  
488 metagenome distance estimation using a rapid primary algorithm (Mash) and average nucleotide  
489 identity (ANI) using dRep version 2.3.2<sup>62</sup> and included in the analysis.

490

#### 491 **Analysis of global oil reservoir microbiome sequences**

492 Raw high-throughput sequence data, totalling 53,019,792 reads from ten separate studies, was  
493 obtained from the National Center for Biotechnology Information's (NCBI) Sequence Read  
494 Archive<sup>63</sup> (SRA) by compiling sequence accession lists and using the SRA Toolkit. Initial  
495 sequence data processing was performed using VSEARCH version 2.11.1<sup>64</sup>. If necessary, paired-  
496 end sequence files were merged based on a minimum overlap length of 10 base pairs (bp) and a  
497 maximum permitted mismatch of 20% of the length of the overlap. Merged reads were filtered  
498 with a maximum expected error of 0.5 for all bases in the read, and minimum and maximum read  
499 lengths of 150 and 500 bp, respectively. Identical reads were dereplicated and annotated with their

500 associated total abundance for each sample, prior to *de novo* chimera detection. Re-replication  
501 resulted in 10,857,433 quality-controlled reads. In addition to these amplicons generated by high-  
502 throughput sequencing platforms, 2,850 near full length amplicon sequences from 49 separate  
503 clone library and/or cultivation-based studies were downloaded from the NCBI's GenBank  
504 database using published accession numbers. Taxonomy was assigned to the combined 10,860,283  
505 sequences using the Ribosomal Database Project's k-mer-based naïve Bayesian classifier with the  
506 Silva database version 138<sup>50</sup>.

507

508 **Statistical analysis and data visualization**

509 Statistical analyses and visualization were performed using base R version 3.6.1<sup>49</sup>, or the specific  
510 R packages described below. Non-metric multidimensional scaling (NMDS) of Bray-Curtis  
511 dissimilarity was calculated using the *metaMDS* function of the *vegan* package<sup>65</sup> in R and  
512 visualized using the *ggplot2* package<sup>66</sup>. Analysis of similarity (ANOSIM) tests measured  
513 significant differences between sediment communities and were performed using the *anosim*  
514 function of the *vegan* package<sup>65</sup>.

515

516 Microbial indicator sequence analysis, designed to test the association of a single ASV with an  
517 environment through multilevel pattern analysis, was used to identify sequences that best represent  
518 specific sediments or groups of sediments under variable test conditions based on both ASV  
519 presence/absence and relative abundance patterns. Indicator ASVs were calculated using the  
520 *multipatt* function of the *indicspecies* package in R, employing a point-biserial correlation index  
521<sup>67</sup>. Tests were performed on amplicon libraries constructed after 28 and 56 days of high  
522 temperature incubation, omitting pre-incubation (day-0) libraries as representing samples prior to

523 endospore enrichment. Among the 32,018 ASVs, only those present in >1% relative abundance in  
524 at least one sample across the entire dataset were included in the analysis. The strength of the  
525 association is represented by the IndicSpecies Stat value (plotted in Fig. 3a). Only observations  
526 with  $P < 0.05$  were considered statistically significant and reported.

527

### 528 **Phylogenetic analysis**

529 ASVs associated with thermogenic hydrocarbons, together with their five most closely related  
530 sequences from Genbank (determined by BLAST searches), were aligned using the web-based  
531 multiple sequence aligner SINA<sup>68</sup>. Aligned sequences were imported into the ARB-SILVA 138  
532 SSU Ref NR 99 database<sup>50</sup> and visualized using the open-source ARB software package<sup>69</sup>. A  
533 maximum likelihood (PhyML) tree was calculated with near full length (>1,300 bases) bacterial  
534 16S rRNA gene reference sequences as well as those from closest cultured isolates. In total, 172  
535 sequences were used to calculate phylogeny (bootstrapped with 1,000 re-samplings), accounting  
536 for 1,006 alignment positions specified based on positional variability and termini filters for  
537 bacteria. Using the ARB Parsimony tool, ASV and Genbank sequences were added to the newly  
538 calculated tree using positional variability filters covering the length of the representative  
539 sequences for each sequence without changing the overall tree topology (Extended Data Fig. 4).  
540 Trees were annotated using iTOL version 5.5<sup>70</sup>.

541

### 542 **Dipicolinic acid (DPA) measurement**

543 Sediment samples were prepared in triplicate using the methods described in Lomstein and  
544 Jørgensen (2012)<sup>71</sup> and Rattray *et al.* (2021)<sup>72</sup>. To extract DPA, 0.1 g of freeze-dried sediment was  
545 hydrolysed by addition of 6M HCl and heating at 95°C for 4 hours, before quenching on ice to

546 stop hydrolysis. The hydrolysate was freeze dried, reconstituted in Milli-Q water, frozen and freeze  
547 dried again. Samples were then dissolved in 1M sodium acetate and aluminium chloride was  
548 added. Sediment extracts were filtered (0.2  $\mu$ m) and mixed with terbium ( $Tb^{3+}$ ) prepared in 1M  
549 sodium acetate. DPA was separated and eluted using gradient chromatography over a Kinetex 2.6  
550  $\mu$ m EVO C18 100 $\text{\AA}$  LC column (150 x 4.5 mm; Phenomenex, USA) fitted with a guard column.  
551 Solvent A was 1M sodium acetate amended with 1M acetic acid to pH 5.6 and solvent B was 80%  
552 methanol: 20% water pumped with a Thermo RS3000 pump (Thermo Scientific Dionex, USA).  
553 The sample injection volume was 50  $\mu$ l and the total run time was 10 min (including flushing).  
554 Detection was performed using a Thermo FLD-3000RS fluorescence detector (Thermo Scientific  
555 Dionex, USA) set at excitation wavelength 270 nm and emission 545 nm. To determine DPA  
556 concentrations under the limit of detection, samples were analysed using standard addition<sup>71</sup>. For  
557 this, a known concentration of DPA standard / $Tb^{3+}$  sodium acetate was sequentially added to the  
558 sediment exact and analysed. Concentrations were calculated using methods described in Lomstein  
559 and Jørgensen (2012)<sup>71</sup>.

560

561 **Data and materials availability** All data is available in the main text or the supplementary  
562 materials. Amplicon and metagenome sequences generated in this study are available through the  
563 NCBI Sequence Read Archive (<https://www.ncbi.nlm.nih.gov>; BioProject accession number  
564 PRJNA604781).

565 **Methods references**

566 42. Campbell, D. C. & MacDonald, A. W. A. CCGS Hudson Expedition 2015-018 Geological  
567 investigation of potential seabed seeps along the Scotian Slope, June 25–July 9, 2015  
568 (Geological Survey of Canada, Open File 8116, 2016).

569 43. Campbell, D. C. CCGS Hudson Expedition 2016-011, phase 2. Cold seep investigations on the  
570 Scotian Slope, offshore Nova Scotia, June 15–July 6, 2016 (Geological Survey of Canada,  
571 Open File 8525, 2019).

572 44. Campbell, D. C. & Normandeau, A. CCGS Hudson Expedition 2018-041: high-resolution  
573 investigation of deep-water seabed seeps and landslides along the Scotian Slope, offshore Nova  
574 Scotia, May 26–June 15, 2018 (Geological Survey of Canada, Open File 8567, 2019).

575 45. Isaksen, M. F., Bak, F. & Jørgensen, B. B. Thermophilic sulfate-reducing bacteria in cold  
576 marine sediment. *FEMS Microbiol. Ecol.* **14**, 1–8 (1994).

577 46. Klindworth, A. et al. Evaluation of general 16S ribosomal RNA gene PCR primers for classical  
578 and next-generation sequencing-based diversity studies. *Nucleic Acids Res.* **41**, 1–11 (2013).

579 47. Martin, M. Cutadapt removes adapter sequences from high-throughput sequencing reads.  
580 *EMBnet J.* **17**, 10–12 (2011).

581 48. Callahan, J. et al. DADA2: High-resolution sample inference from Illumina amplicon data.  
582 *Nat. Methods* **13**, 581–583 (2016).

583 49. R Core Team, R: A language and environment for statistical computing. (R Foundation for  
584 Statistical Computing, Vienna, Austria, 2014); [www.R-project.org/](http://www.R-project.org/).

585 50. Quast, C. et al. The SILVA ribosomal RNA gene database project: improved data processing  
586 and web-based tools. *Nucl. Acids Res.* **41**, 590–596 (2013).

587 51. McMurdie, P. J. & Holmes, S. Phyloseq: an R package for reproducible interactive analysis  
588 and graphics of microbiome census data. *PLoS One* **8**, (2013).

589 52. Li, D., Liu, C-M., Luo, R., Sadakane, K. & Lam, T-W. MEGAHIT: An ultra-fast single-node  
590 solution for large and complex metagenomics assembly via succinct de Bruijn graph.  
591 *Bioinformatics* **31**, 1674–1676 (2015).

592 53. Kang, D. D. et al. MetaBAT 2: an adaptive binning algorithm for robust and efficient genome  
593 reconstruction from metagenome assemblies. *PeerJ* **7** (2019).

594 54. Parks, D. H., Imelfort, M., Skennerton, C. T., Hugenholtz, P. & Tyson, G. W. CheckM:  
595 Assessing the quality of microbial genomes recovered from isolates, single cells, and  
596 metagenomes. *Genome Res.* **25**, 1043–1055 (2015).

597 55. Gruber-Vodicka, H., Pruesse, E. & Seah, B. K. B. phyloFlash – Rapid SSU rRNA profiling  
598 and targeted assembly from metagenomes. *mSystems* **5**, 1–16 (2017).

599 56. Dong, X. & Strous, M. An integrated pipeline for annotation and visualization of metagenomic  
600 contigs. *Front. Genet.* **10** (2019).

601 57. Graham, E. D., Heidelberg, J. F. & Tully, B. J. Potential for primary productivity in a globally-  
602 distributed bacterial phototroph. *ISME J.* **350**, 1–6 (2018).

603 58. Kanehisa, M., Sato, Y. & Morishima, K. BlastKOALA and GhostKOALA: KEGG tools for  
604 functional characterization of genome and metagenome sequences. *J. Mol. Biol.* **428**, 726–731  
605 (2016).

606 59. Hyatt, D. et al. Prodigal: Prokaryotic gene recognition and translation initiation site  
607 identification. *BMC Bioinformatics* **11**, 119 (2010).

608 60. Chaumeil, P. A., Mussig, A. J., Hugenholtz, P. & Parks, D. H. GTDB-Tk: A toolkit to classify  
609 genomes with the Genome Taxonomy Database. *Bioinformatics* **36**, 1925–1927 (2019).

610 61. Schloss, P. D. et al. Introducing mothur: Open-Source, platform-independent, community-  
611 supported software for describing and comparing microbial communities. *Appl. Environ.*  
612 *Microbiol.* **75**, 7537–7541 (2009).

613 62. Olm, M. R., Brown, C. T., Brooks, B. & Banfield, J. F. dRep: a tool for fast and accurate  
614 genomic comparisons that enables improved genome recovery from metagenomes through de-  
615 replication. *ISME J.* **11**, 2864–2868 (2017).

616 63. Leinonen, R., Sugawara, H. & Shumway, M. The Sequence Read Archive. *Nucleic Acids Res.*  
617 **39**, 19–21 (2011).

618 64. Rognes, T., Flouri, T., Nichols, B., Quince, C. & Mahé, F. VSEARCH: a versatile open source  
619 tool for metagenomics. *PeerJ* **4**, 1–22 (2016).

620 65. Oksanen, J., Kindt, R., Legendre, P. & O'Hara, B. *The Vegan Package—Community Ecology*  
621 *Package. R package version 2.0-9* (2007).

622 66. Wickham, H. *ggplot2: Elegant Graphics for Data Analysis* (Springer, New York, 2009);  
623 <http://ggplot2.org>.

624 67. De Cáceres, M., Legendre, P. & Moretti, M. Improving indicator species analysis by  
625 combining groups of sites. *Oikos* **119**, 1674–1684 (2010).

626 68. Pruesse, E., Peplies, J. & Glöckner, F. O. SINA: Accurate high-throughput multiple sequence  
627 alignment of ribosomal RNA genes. *Bioinformatics* **28**, 1823–1829 (2012).

628 69. Ludwig, W. et al. ARB: a software environment for sequence data. *Nucleic Acids Res.* **32**,  
629 1363–1371 (2004).

630 70. Letunic, I. & Bork, P. Interactive Tree of Life (iTOL) v4: recent updates and new  
631 developments. *Nucleic Acids Res.* **47**, 256–259 (2019).

632 71. Lomstein, B. A. & Jørgensen, B. B. Pre-column liquid chromatographic determination of

633 dipicolinic acid from bacterial endospores. *Limnol. Oceanogr. Methods* **10**, 227–233 (2012).

634 72. Rattray, J. E. et al. Sensitive quantification of dipicolinic acid from bacterial endospores in

635 soils and sediments. *Environ. Microbiol.* **23**, 1397–1406 (2021).

636 **Acknowledgements** We wish to thank the crew of CCGS *Hudson* and Natural Resources Canada  
637 for collection of piston cores and onboard core processing. Ship time funding and support was  
638 provided by the Nova Scotia Department of Energy and Mines, the Nova Scotia Offshore Energy  
639 Research Association, and Natural Resources Canada. The authors wish to thank Steve Larter,  
640 Lisa Gieg, Bo Barker Jørgensen and Rhonda Clark for helpful discussions and suggestions and  
641 research support.

642

643 **Author contributions** C.R.J.H. and A.M. secured research funding. P-A.D, N.M., D.C.C. and  
644 A.M. acquired, processed and analyzed geophysical data. D.A.G., A.C., C.L., M.A.C., J.W., A.M.,  
645 D.C.C. and C.R.J.H. collected and processed marine sediment samples for testing. M.F., J.W. and  
646 D.A.G. generated and analyzed hydrocarbon geochemical data. D.A.G., A.C., C.L., O.H., M.A.C.  
647 and C.R.J.H generated, processed and interpreted microbial community data. D.A.G. and S.B.  
648 curated and analyzed reservoir microbiome data. D.A.G. and J.Z. processed and analyzed  
649 metagenomic data. J. R. measured and interpreted DPA signals. D.A.G. and C.R.J.H. drafted the  
650 manuscript with feedback from all authors during refinement and finalization.

651

652 **Competing interests** The authors declare no competing interests.

653

654 **Additional information**

655 **Funding** This work was supported by a Mitacs Accelerate Fellowship awarded to D.A.G., and by  
656 a Genome Canada Genomics Applications Partnership Program grant facilitated by Genome  
657 Atlantic and Genome Alberta awarded to C.R.J.H and A.M., and a Canada Foundation for

658 Innovation grant (CFI-JELF 33752) for instrumentation, and Campus Alberta Innovates Program

659 Chair funding awarded to C.R.J.H.

660 **Correspondence and requests for materials** can be addressed to D.A.G. and C.R.J.H.